Latitudinal shift of the Atlantic Meridional Overturning Circulation source regions under a warming climate

Camille Lique, Matthew D. Thomas

nature climate change

ARTICLES

https://doi.org/10.1038/s41558-018-0316-5

Latitudinal shift of the Atlantic Meridional Overturning Circulation source regions under a warming climate

Camille Lique[1*] and Matthew D. Thomas[2]

The strength of the Atlantic Meridional Overturning Circulation, a key indicator of the climate state, is maintained by the subduction of dense water that feeds the deep southwards branch. At present, this subduction occurs almost entirely in the subpolar region, in the Labrador, Irminger and Nordic seas; however, whether this will continue under climate change is unknown. Here we use a quantitative Lagrangian diagnostic applied to climate model output to show that, in response to warming, the main source regions of this mixed-layer subduction shift northwards to the Arctic Basin and southwards to the subtropical gyre. These shifts are explained by changes in background stratification, mixed-layer depth and ocean circulation, highlighting the need to consider the full three-dimensionality of the circulation and its changes to accurately predict the future climate state.

The Atlantic Meridional Overturning Circulation (AMOC) is a key element of the global climate system. The northward transport of heat associated with the surface branch of the AMOC contributes, for instance, to the mild climate of western Europe[1], which is estimated to be around 5 °C warmer than it would otherwise be. Continuous monitoring of the AMOC strength across the RAPID array at 26° N or the OVIDE line between Portugal and Greenland has captured a decline over the past two decades[2,3], and recent proxy reconstructions have revealed that it is at its weakest state for the past few hundred years[4,5]. More generally, long-term changes in the AMOC strength are thought to be a good indicator of climate change[6]. As such, the changes in the AMOC simulated by a series of coupled climate models forced with a range of increasing greenhouse gas emission scenarios have been investigated as part of the different phases of the Climate Model Intercomparison Project (CMIP[7]). While discrepancies between the different model ensemble members remain large, all predict a decline in AMOC strength. On average, it is projected to decrease by 25%–30% by 2100 (for CMIP3 models under scenario A1B[8], and CMIP5 models provide qualitatively similar predictions[9]). Using simulations based on a low-resolution coupled climate model (CCSM4) forced by different emission scenarios, the relationship between projected change in AMOC strength and level of CO_2 in the atmosphere has been rationalized, suggesting that the simulated decrease of strength is proportional to the transient CO_2 forcing (once interannual variability is smoothed out)[10].

There is a large body of literature focusing on measuring, modelling and understanding the AMOC and its variability and long-term changes (see ref. [11] and references therein). Yet, a full mechanistic understanding of what drives the AMOC variability is still needed to reduce the uncertainty associated with the prediction of its future changes. It is widely recognized that a large part of the AMOC seasonal and interannual variability is driven by winds[12], while changes on longer timescales probably involve a complex interplay between wind- and buoyancy-driven processes[13]. Various modelling studies have linked decadal variability of the AMOC strength with the intensity of deep convective events occurring in the Labrador Sea[14] or the Irminger Sea[15], and the intensity of the Denmark Strait overflow[16], which is fed upstream by deep convection in the Greenland Sea and the Arctic Basin[17]. Predicting the potential changes in intensity and location of deep convection, and its contribution to AMOC, under a warming climate is thus of utmost importance to predict the future evolution of the global climate system.

A recently developed methodology[18], based on Lagrangian particle tracking applied to model outputs, allows an exact determination of the contribution to the AMOC from subduction at the base of the mixed layer in different regions. Here we use this methodology to investigate the relative regional contributions in a coupled climate model and to assess how it changes under a warming climate. This is motivated by the finding that deep convection in the Arctic Basin could emerge under a warming climate[19]. Therefore, some regions, such as the Arctic, might exert an increasingly important control on the AMOC in the future.

Source region changes

To investigate the link between the region of deep convection and the intensity of the AMOC, we examine the time series of the AMOC strength, computed in two simulations performed with the Centre National de Recherches Météorologiques (CNRM) climate model[20] forced with constant concentrations of atmospheric CO_2 representative of pre-industrial conditions (CTRL), and strong global warming conditions ($4\times CO_2$) (see Methods for more details). However, as for all of the state-of-the-art fully coupled climate models, the ocean component of the CNRM model is too low resolution to explicitly resolve mesoscale eddies and small-scale features, which might be important processes for mixed-layer subduction[21] or the AMOC[22]. Here, we define the AMOC as the maximum of the zonally and depth-integrated transport along the latitude of the RAPID array at 26° N, to allow direct comparison against observational estimates. In the CTRL run, the mean and standard deviation of the annual mean time series are 14.2 Sv and 0.8 Sv, respectively (Fig. 1). This is weaker than the 17.2 Sv observed from the RAPID array for the period 2004–2012[2], but within the range of values simulated by the CMIP5 models (between 10 and 21 Sv[23]). In the $4\times CO_2$

[1]IFREMER, Univ. Brest, CNRS, IRD, LOPS, Plouzané, France. [2]Department of Geology and Geophysics, Yale University, New Haven, CT, USA.
*e-mail: camille.lique@ifremer.fr

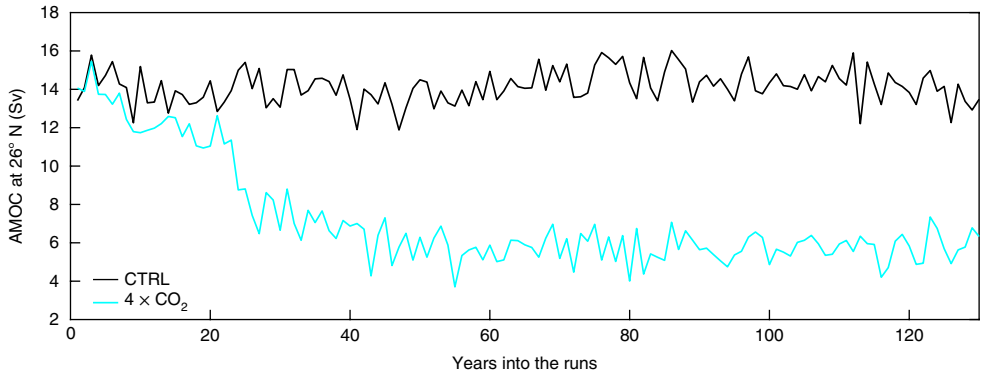

Fig. 1 | AMOC strength at 26° N in CTRL and 4 × CO_2. The lines show the time series of the AMOC (in Sv, defined as the maximum of the zonally and depth-integrated transport along the RAPID section at 26° N) for the two simulations used in this study (CTRL in black and 4 × CO_2 in blue).

simulation, the AMOC strength shows a sharp decline during the first 50 years, corresponding to the adjustment period to increased atmospheric CO_2, before equilibrating and oscillating around a mean value of 5.7 Sv. This ~60% decrease compared to the CTRL run is consistent with (although slightly larger than) that found in CMIP5 models under RCP8.5 forcing[9].

A Lagrangian analysis is performed to determine the geographical origin of the water mass flowing southward within the deeper branch of the AMOC at 10° N (see Methods). Figure 2 summarizes the integrated contributions of mixed-layer subduction from different regions to the vertical structure of the AMOC reconstructed at 26° N. In the CTRL simulation, the largest contribution is subduction occurring in the subpolar region (9.5 Sv), while smaller contributions arise from the Nordic Sea (1.9 Sv), the subtropical gyre (1.4 Sv, including 0.1 Sv from the Mediterranean Sea) and the Arctic Basin (1 Sv in total, including 0.9 Sv from the Barents Sea alone). The integrated subpolar region contribution is the sum of contributions from the Labrador Sea (3.6 Sv), the Irminger Sea (3.3 Sv) and the Rockall Basin (2.6 Sv). These model estimates can be compared to previous observational estimates of subduction in the Labrador (2 Sv)[24], Irminger (3.2 Sv)[25] and Nordic (5.6 Sv corresponding to Denmark Strait overflows)[26] seas. Although the CTRL run estimates and observations are similar, it is clear that the model tends to: overestimate the contribution corresponding to open-ocean convection south of the Greenland–Scotland Ridge, which is a common bias of most coupled climate models, making it difficult to link directly variations of the intensity of deep convection and AMOC strength[23]; and underestimate the component formed north of it and further cascading of dense water. Note that the latter also encompasses Arctic Basin subduction, where dense waters form and are eventually exported to the Greenland Sea through Fram Strait[17]. The significant contribution from subduction in the subtropical gyre is also consistent with the 2 Sv estimated through a combination of observations, model results and theory[27].

A very different picture emerges from the 4 × CO_2 run (Fig. 2b). In this case, the contribution from mixed-layer subduction in the subpolar region nearly collapses (0.2 Sv in total, with ~75% from the Irminger Sea). The Nordic Sea contribution also reduces (0.9 Sv). In contrast, new large contributions emerge at both lower and higher latitudes. In the 4 × CO_2 run, subduction occurring in the Arctic region sustains a significant part of the AMOC (1.7 Sv). Given the tendency of the CNRM model to promote open-ocean convection over cascading of dense water in the CTRL run, and assuming that the same bias exists in the 4 × CO_2 run, we expect that the model would also tend to underestimate the future contributions from subduction north of the Greenland–Scotland Ridge (that is, the contributions from the Nordic Sea and the Arctic Basin). Finally, the subtropical region contribution now accounts for 3.5 Sv, more than half of the total AMOC at 26° N. This contribution largely determines the vertical structure of the weakened AMOC, with a maximum transport peaking at 100 m, compared to the maximum AMOC transport depth of ~900 m in both the CTRL run and RAPID observations (Fig. 2a). This shoaling in response to a strong decrease of the AMOC strength has been documented in climate models[28], and was linked to the reduction of dense water formation in the North Atlantic. The same processes are most likely at play in our 4 × CO_2 simulation, suggesting that a change in the vertical AMOC structure is, in addition to a signature of a density change in the deeper branch, partly a signature of the changes in the relative importance of the contributing regions.

Conditions for change

To determine what circumstances led to a latitudinal shift of the contributing regions in the 4 × CO_2 run, we examined the spatial and temporal distribution of the mixed-layer subduction in the two simulations, in relation to the regional ocean conditions. Figure 3 compares the 60-year March climatology mixed-layer depth (MLD) in the CTRL and 4 × CO_2 simulations, as well as Lagrangian estimates for the mixed-layer subduction rates (Sr) that directly contribute to the AMOC. Sr is estimated at each model grid point, and corresponds to the transport of the particles initiated at 10° N that, when integrated backward in time, intercept the base of the mixed layer (see Methods). The spatial pattern of Sr broadly follows the March climatology MLD pattern (Fig. 3). This is expected, as most of the transfer from the mixed layer to the interior is thought to occur in March, when the mixed layer is deepest and starts shoaling again (a process known as 'Stommel's mixed-layer demon'[29]). Yet, the two quantities are not fully equivalent (for example, the deepest MLD and the highest subduction rates do not always coincide), due to the different nature of the diagnostics. Indeed, a deeper MLD does not necessarily translate into a larger contribution to the deeper branch of the AMOC as the link between MLD and higher subduction rate is modulated by the timing, location and environment conditions of where the MLD varies. Moreover, Sr captures only the water masses that subduct at the base of the mixed layer and eventually cross southwards at 10° N, neglecting any contribution from water masses first obducting again into the mixed layer of the North Atlantic or the Arctic Basin.

To investigate the potential drivers of the MLD and Sr changes between the two simulations, we relate them to the background oceanic conditions and their changes according to an estimation of the stratification[30] (Fig. 4). To first order, mixed layers have the potential to deepen more where the background stratification is weaker[23]. In the CTRL simulation, the deepest MLD and highest Sr are found in

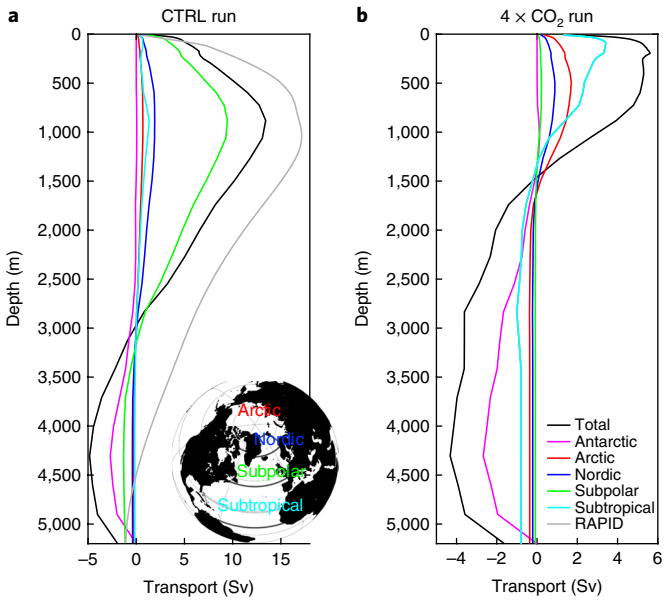

Fig. 2 | Regional contributions to the AMOC streamfunctions at 26° N. a,**b**, The mean AMOC depth profile at 26° N for the CTRL (**a**) and $4\times CO_2$ (**b**) simulations. The total is indicated in black, as well as the different contributions from mixed-layer subduction in the different regions indicated in the inserted map, obtained from the Lagrangian analysis. Note that the *x* axes are different between the two panels. The computation has been performed with additional sub-regions discussed in the text, but omitted for the sake of clarity. The Antarctic contribution corresponds to the transport associated with all of the particles recirculating within the domain without interacting with the mixed layer, while the contribution that comes directly from Bering (and does not first interact with the mixed layer) is small. The light grey line in **a** shows the AMOC estimate from observations at the RAPID array (averaged over the period 2004–2012) and the light grey line on the map indicates the position of the RAPID section at 26° N.

the subpolar region, and more specifically close to the sea ice edge, in the Labrador Sea to the south of Cape Farewell and on the Rockall plateau north of Scotland (Fig. 3a,c). In the subpolar region, the stratification is generally weak (Fig. 4a), providing a favourable preconditioning for the mixed layer to deepen in winter in response to atmospheric forcing. Overall, the magnitude and general pattern of MLD are in broad agreement with climatology based on observations (see Supplementary Fig. 1) as well as results from CMIP5 control simulations[31]. The main model bias is the too large depths and the too large southwestward extension of the Labrador Sea convective patch. South of Denmark Strait, Sr also reaches a peak of 900 m yr^{-1}, although the MLD does not exceed 500 m in this region. This mismatch between MLD and Sr is probably due to the entrainment of surrounding water by the overflow in this region, which contributes significantly to the deeper branch of the AMOC[32]. South of Svalbard, the convective patch (and the associated Sr) spreads to the mean ice-covered region (Fig. 3a). This is the signature of interannual variations in the sea ice edge location, as deep convection occurs during years with lower sea ice extent[33]. Closer to the Greenland coast and in the Arctic Basin, the stratification is strong (Fig. 4a) due to strong vertical salinity gradients within the fresh surface layer. Moreover, the presence of sea ice inhibits exchange with the atmosphere and results in shallow mixed layers (Fig. 3a). These findings are in agreement with observations[34] and model simulations[19].

In the subtropical region, mixed layers do not exceed 300 m despite the weak background stratification. While weak stratification is a necessary condition for deep convection to occur, it alone is not sufficient and other factors, such as high-frequency variations of the atmospheric forcing, have been shown to be required to trigger convective events[35]. A local MLD maximum (~300 m) is found on the western side of the gyre, characteristic of the presence of 18 °C mode water[36]. In this region, Sr does not exceed 50 m yr^{-1}, in agreement with observations[37]. The region of small Sr values spans most of the subtropical gyre, resulting in a small, yet significant integrated subtropical contribution to the AMOC (Fig. 2a). This contribution has previously been identified as the wind-driven subtropical cell[27], suggesting the existence of an interior 'exchange window' for the water mass subducted on the eastern side of the subtropical gyre[38]. In addition to the surface subtropical cell, our results suggest the existence of a deeper and longer path of water masses subducted at the base of the mixed layer in the subtropical regions, which flows in the subsurface layer further north (up to 50–60° N) before returning at depth to the south (see Supplementary Fig. 2). This may represent a component of the subsurface ocean connection proposed to exist between the subtropical and subpolar gyres[39]. Finally, Sr also exhibits a local maximum immediately northwest of our seeding section at 10° N (Fig. 3c), which corresponds to very shallow water masses circulating within the surface layer of the subtropical gyre and reaching the section at 10° N within a few months of subduction without contributing significantly to the integrated mid-depth contribution of the subtropical region to the AMOC.

Compared to the CTRL run, winter MLD and subduction rate are generally much shallower and weaker in the $4\times CO_2$ simulation (Fig. 3b,d). In the subpolar gyre, where MLDs are the deepest in the CTRL run, MLD does not exceed 200 m anywhere, and subduction rates are consequently mostly negligible. The strong winter MLD shoaling in the subpolar region indicates the cessation of deep convection, a common feature of climate models under future radiative forcing[31]. Accordingly, the stratification in the subpolar region is also stronger in the $4\times CO_2$ run than in the CTRL simulation (Fig. 4b), due to increased salinity gradients in this region (not shown). Various factors have been proposed for the increased stratification, including atmospheric warming[40] or freshening of the surface layer due to increased freshwater exports from the Arctic[10]. The changes in stratification seen in Fig. 4c are in agreement with changes predicted by CMIP3 models[30], although the changes simulated by the CNRM model tend to be stronger, probably because our radiative scenario is stronger.

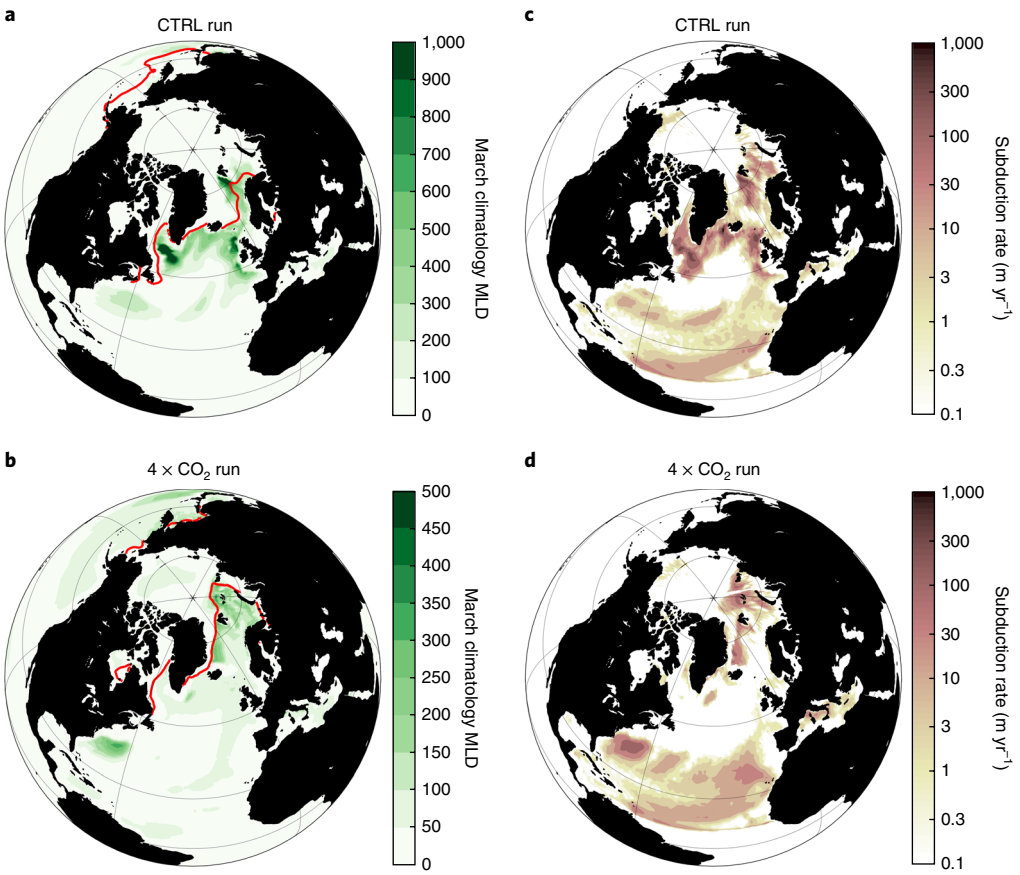

Fig. 3 | Changes in MLD and subduction rates. a,**b**, March climatology MLD for the CTRL (**a**) and the $4\times CO_2$ (**b**) runs. The red contour corresponds to the location of the sea ice edge (defined as the 15% concentration contour). **c**,**d**, Mixed-layer subduction rates, as determined from the Lagrangian analysis performed on the CTRL (**c**) and the $4\times CO_2$ (**d**) runs, for water parcels tracked backward in time from a section at 10º N in the Atlantic to the base of the mixed layer. Note that the colour bars in **a** and **b** are different, and that the scale used in **c** and **d** is nonlinear.

In the Arctic Basin and the Nordic Sea, where the density (and thus the stratification) is primarily determined by the salinity, as in any cold environment, the sign of the stratification change in the $4\times CO_2$ run is different depending on the region considered. In the Canadian Basin, it is strongly enhanced and on the Eurasian side of the Arctic and the Nordic Sea, it is strongly reduced (Fig. 4c). The map of stratification changes in the CNRM model is very similar to the pattern found in a different climate model[19], where changes are due to a redistribution of the Arctic freshwater content between the basins from a change in the wind-driven circulation. As sea ice cover is reduced under a warming climate, the wind input of momentum to the ocean increases, and thus spins up the Beaufort Gyre (where freshwater is accumulated) and enhances the propagation of warm and salty Atlantic water on the Eurasian side of the Arctic. This causes the winter mixed layer in the Eurasian Basin to deepen significantly[19]. The same mechanism is probably at play in the CNRM model since the Arctic Basin is seasonally ice-free in the $4\times CO_2$ simulation, the winter sea ice extent is greatly reduced (Fig. 3c) and the change in barotropic streamfunction (that is, the integrated transport from the surface to the bottom of the ocean) indicates a spin up of the surface circulation (Fig. 4f). The March mixed layer deepens to ~300–400 m on average along the sea ice edge in the Eurasian Basin and the Barents and Nordic seas (Fig. 3), and reaches as deep as 800 m in the Arctic during certain years (not shown). This deepening of the mixed layer is also accompanied by increased Sr (Fig. 3d), resulting in a larger contribution of these regions to the AMOC (Fig. 2b).

In the subtropical region, the spatial pattern of the subduction rates estimated from the particles tracked in the $4\times CO_2$ run is broadly similar to that in the CTRL simulation, although the values are generally higher (Fig. 3d). In contrast to the higher latitudes, the changes in Sr are not reflected in the changes in MLD or stratification. On the western side of the basin, the MLD patch corresponding to mode water formation tends to shrink in response to increased stratification of the upper ocean (Fig. 4b,c). Similar projected weakening of mode water formation has been documented in the Pacific subtropical gyre[41]. Yet, despite shoaling of the mixed layer, Sr increases. We suggest that this is not caused by an increase in subtropical subduction rates under climate change, but because of a change in the fate of the water subducted here (see Supplementary Figs. 2 and 3). The connectivity between the Atlantic subtropical and subpolar gyres has been suggested to be strongest in the subsurface ocean at the depth of the main thermocline, rather than at the surface[39]. After descending to this depth under the action of Ekman pumping, the water can flow isopycnally northwards and upwards towards the surface of the subpolar ocean. However, in the $4\times CO_2$ run, the enhanced subpolar stratification (Fig. 4b,c) inhibits the surface outcropping, perhaps suggesting that the subtropical-ventilated water must recirculate at depth. With a much shallower overturning cell in the $4\times CO_2$ run, the subtropical component can thereby contribute more directly to the overturning. There may also be a link between the vertical (overturning) circulation and the horizontal circulation, which strongly spins down in the subtropical gyre under climate forcing (Fig. 4e,f). The increased importance of

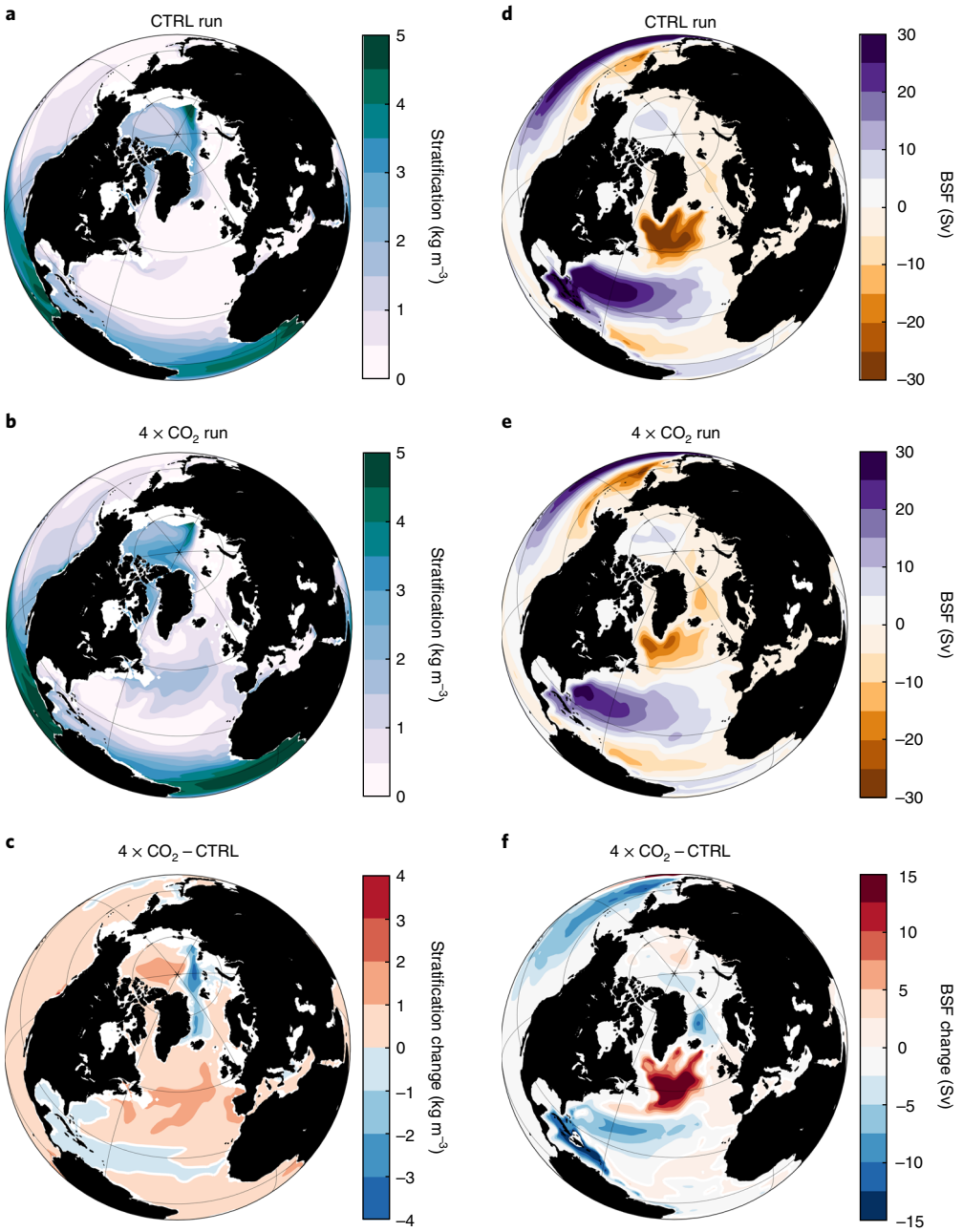

Fig. 4 | Changes in stratification and gyre circulation. a–f, March climatology stratification (**a**,**b**; defined as the density difference between 200 m and the surface), mean barotropic streamfunction (**d**,**e**; BSF) for the CTRL and the 4 × CO_2 runs and the difference between the two runs (**c**,**f**).

the subduction of subtropical water may help determine the vertical structure of the AMOC in the 4 × CO_2 run, which undergoes a large shoaling of the deeper branch as subducting waters become less dense (Fig. 2b).

Concluding discussion

Year-to-year variations of the observed MLD in the convective regions of the subpolar gyre have been scrutinized for decades[42–44], on the basis of the premise that the AMOC lower limb is fed by dense water formed in these regions, and thus MLD variation is a good predictor of AMOC variability[23]. On the basis of this axiom, projected changes in MLD under a warming climate have also been investigated[31,40]. This assumes, however, that the mechanisms that set the strength of the AMOC in present-day conditions would not change when transitioning to a warmer climate. Our results question this paradigm. Using simulations from the CNRM climate model, we suggest that, in addition to the large decrease of the AMOC strength under a warming climate, the mechanisms could change, as the regions where mixed-layer subduction contributes significantly to the AMOC may shift (Fig. 5). Indeed, while the AMOC is, as expected, almost entirely sustained by mixed-layer subduction in the subpolar gyre in the simulation representative of present-day conditions, subduction in the subtropical gyre and the Arctic Basin become increasingly important in response to a strong increase in atmospheric CO_2 concentrations. The shoaling of the AMOC deeper branch under a warming climate consistently projected by other coupled models[28] might be a strong indication that the AMOC becomes increasingly driven by subduction in the subtropical gyre in those models as well. While projected Arctic sea ice decline is widely thought to trigger a weakening of the

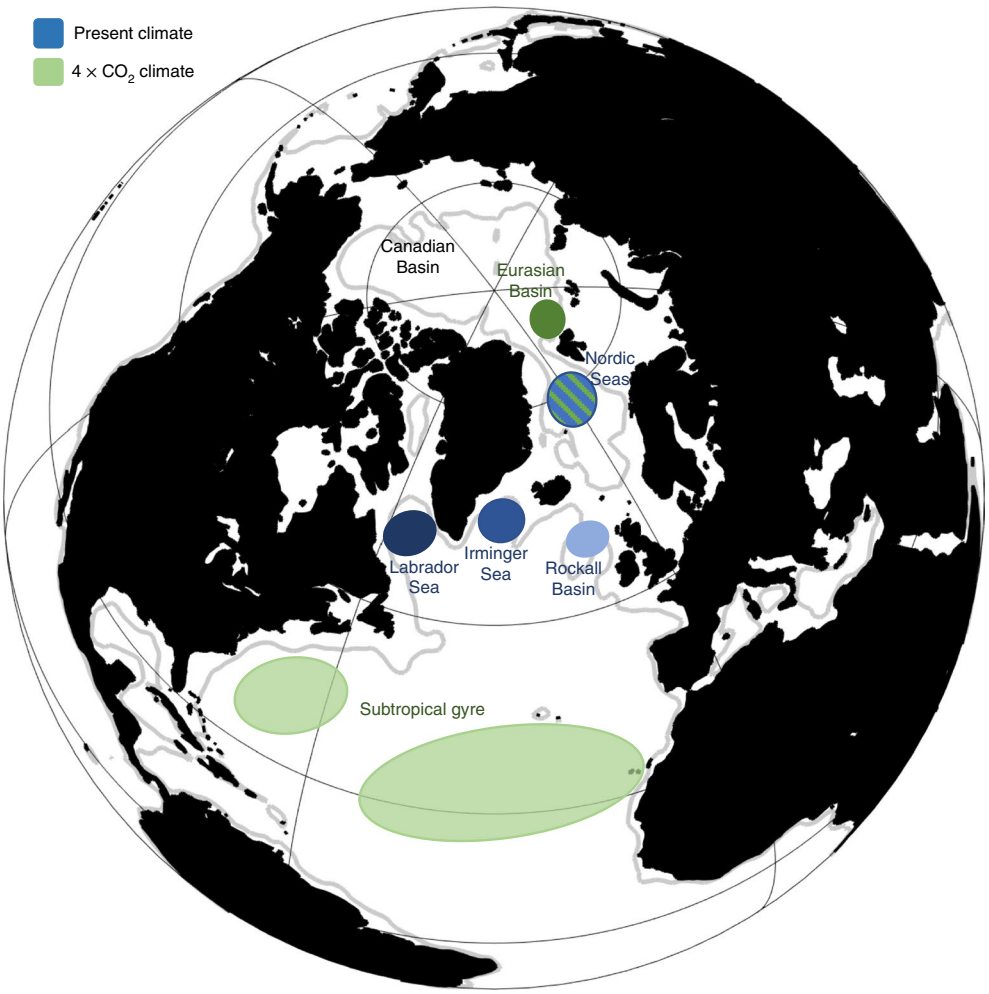

Fig. 5 | Changes in the dominant source regions of the AMOC deep limb. Schematic diagram illustrating the latitudinal shift of the regions where mixed-layer subduction contributes to the AMOC under a warming climate. The blue patches correspond to regions contributing the most to the AMOC in our present climate, while the green patches show these regions for the future warmer climate. Darker colours indicate regions where deeper mixed layer are found. The grey line indicates the 1,500 m isobath.

AMOC[10,45], our results point to a new possible interplay between AMOC strength and changes in the Arctic. Indeed, as the winter sea ice extent shrinks, deep convection can emerge in the Arctic Basin itself[19], resulting in a new and significant subduction contribution to the AMOC.

Our model results suggest that the regional increase in mixed-layer subduction occurs concomitantly with a change in the wind-driven surface circulation. In the $4\times CO_2$ simulation, the subtropical gyre spins down, in agreement with the hypothesized future weakening of the Gulf Stream[46]. Meanwhile, the contribution of the subtropical cell subduction to the AMOC increases, suggesting that either the wind- and buoyancy-driven circulations are connected, or more subtropical ventilated water can contribute to the AMOC without first outcropping in the subpolar gyre. In the Arctic Basin, spin up of the Beaufort Gyre leads to a redistribution of the freshwater content between the Canadian and Eurasian basins, resulting in a suppression of the stratification on the Eurasian side and the emergence of deep convection[19]. Overall, our results highlight that horizontal and vertical circulations have to be examined in conjunction to understand the variability and long-term changes in the AMOC.

In reality, the picture might be even more complex than is captured by the CNRM model. For instance, the model does not include any dynamical representation of the Greenland Ice Sheet and thus the effect of its melting under a warming climate is not directly considered here. While results from CMIP5 models generally suggest that the effect of Greenland Ice Sheet melting on the AMOC future decline is of secondary importance[47], including the details of such freshwater release in our model could, to some extent, alter the integrated regional contributions to the AMOC. In particular, it would probably further reduce the subpolar contribution under a warming climate, as increased melt is mainly expected to impact the Labrador Sea and the subpolar region[48]. Furthermore additional small-scale processes (that are only parameterized in the CNRM model) might play a key role in setting the dynamical link between mixed-layer subduction and AMOC. Indeed, resolving mesoscale eddies would probably modify the modelled convective processes (and thus the MLDs and properties[22]) or the spreading of tracers associated with mixed-layer subduction[21]. Moreover, the use of a higher-resolution ocean model could allow a better representation of the dense overflows and thus the AMOC[22]. What is less clear, however, is how small-scale features would differently modify the response of various geographical sources of deep water to climate change. This should be addressed in future studies based on climate models run at higher resolution and including more complexity (such as an interactive ice sheet component).

Finally, our results may have implications for heat and carbon uptake in the context of climate change. Previous studies have pointed out the importance of the change in MLD[49], the AMOC depth extension[28], the AMOC strength[50] or the horizontal circulation[51] to determine the rate of ocean heat and carbon uptake. Similarly, in the CNRM model, all of those processes appear to respond strongly to the increased atmospheric CO_2, suggesting that these rates are probably changing as well. Moreover, the latitudinal shift of the regions where mixed-layer subduction contributes to the AMOC documented here imply that subduction might occur in regions with different air–sea heat and carbon flux under a warming climate, which might also contribute to the rate of the ocean heat and carbon uptake.

Online content

Any methods, additional references, Nature Research reporting summaries, source data, statements of data availability and associated accession codes are available at https://doi.org/10.1038/s41558-018-0316-5.

Received: 4 May 2018; Accepted: 25 September 2018;
Published online: 22 October 2018

References

1. Jackson, L. C. et al. Global and European climate impacts of a slowdown of the AMOC in a high resolution GCM. *Clim. Dynam.* **45**, 3299–3316 (2015).
2. McCarthy, G. et al. Measuring the Atlantic meridional overturning circulation at 26° N. *Prog. Oceanogr.* **130**, 91–111 (2015).
3. Mercier, H. et al. Variability of the meridional overturning circulation at the Greenland–Portugal OVIDE section from 1993 to 2010. *Prog. Oceanogr.* **132**, 250–261 (2015).
4. Caesar, L., Rahmstorf, G. F. S., Robinson, A. & Saba, V. Observed finger-print of a weakening Atlantic Ocean overturning circulation. *Nature* **556**, 191–196 (2018).
5. Thornalley, D. J. R. et al. Anomalously weak Labrador Sea convection and Atlantic overturning during the past 150 years. *Nature* **556**, 227–230 (2018).
6. IPCC *Climate Change 2013: The Physical Science Basis* (eds Stocker, T. F. et al.) (Cambridge Univ. Press, 2013).
7. Taylor, K. E., Stouffer, R. J. & Meehl, G. A. An overview of CMIP5 and the experiment design. *Bull. Am. Meteorol. Soc.* **93**, 485–498 (2012).
8. Schmittner, A., Latif, M. & Schneider, B. Model projections of the North Atlantic thermohaline circulation for the 21st century assessed by observations. *Geophys. Res. Lett.* **32**, L23710 (2005).
9. Cheng, W., Chiang, J. C. & Zhang, D. Atlantic meridional overturning circulation (AMOC) in CMIP5 models: RCP and historical simulations. *J. Clim.* **26**, 7187–7197 (2013).
10. Jahn, A. & Holland, M. M. Implications of Arctic sea ice changes for North Atlantic deep convection and the meridional overturning circulation in CCSM4-CMIP5 simulations. *Geophys. Res. Lett.* **40**, 1206–1211 (2013).
11. Buckley, M. W. & Marshall, J. Observations, inferences, and mechanisms of the Atlantic Meridional Overturning Circulation: A review. *Rev. Geophys.* **54**, 5–63 (2016).
12. Pillar, H. R., Heimbach, P., Johnson, H. L. & Marshall, D. P. Dynamical attribution of recent variability in Atlantic overturning. *J. Clim.* **29**, 3339–3352 (2016).
13. Polo, I., Robson, J., Sutton, R. & Balmaseda, M. A. The importance of wind and buoyancy forcing for the boundary density variations and the geostrophic component of the AMOC at 26°N. *J. Phys. Oceanogr.* **44**, 2387–2408 (2014).
14. Medhaug, I., Langehaug, H. R., Eldevik, T., Furevik, T. & Bentsen, M. Mechanisms for decadal scale variability in a simulated Atlantic meridional overturning circulation. *Clim. Dynam.* **39**, 77–93 (2012).
15. Deshayes, J. & Frankignoul, C. Simulated variability of the circulation in the North Atlantic from 1953 to 2003. *J. Clim.* **21**, 4919 (2008).
16. Lohmann, K. et al. The role of subpolar deep water formation and Nordic Seas overflows in simulated multidecadal variability of the Atlantic meridional overturning circulation. *Ocean Sci.* **10**, 227–241 (2014).
17. Moat, B. I., Josey, S. A. & Sinha, B. Impact of Barents Sea winter air–sea exchanges on Fram Strait dense water transport. *J. Geophys. Res.* **119**, 1009–1021 (2014).
18. Thomas, M. D., Tréguier, A.-M., Blanke, B., Deshayes, J. & Voldoire, A. A Lagrangian method to isolate the impacts of mixed layer subduction on the meridional overturning circulation in a numerical model. *J. Clim.* **28**, 7503–7517 (2015).
19. Lique, C., Johnson, H. L. & Plancherel, Y. Emergence of deep convection in the Arctic Ocean under a warming climate. *Clim. Dynam.* **50**, 3849–3851 (2018).
20. Voldoire, A. et al. The CNRM-CM5. 1 global climate model: description and basic evaluation. *Clim. Dynam.* **40**, 2091–2121 (2013).
21. MacGilchrist, G. A., Marshall, D. P., Johnson, H. L., Lique, C. & Thomas, M. Characterizing the chaotic nature of ocean ventilation. *J. Geophys. Res. Oceans* **122**, 7577–7594 (2017).
22. Marzocchi, A. et al. The North Atlantic subpolar circulation in an eddy-resolving global ocean model. *J. Mar. Syst.* **142**, 126–143 (2015).
23. Heuzé, C. North Atlantic deep water formation and AMOC in CMIP5 models. *Ocean Sci.* **13**, 609–622 (2017).
24. Pickart, R. S. & Spall, M. A. Impact of Labrador Sea convection on the North Atlantic meridional overturning circulation. *J. Phys. Oceanogr.* **37**, 2207–2227 (2007).
25. Sarafanov, A. et al. Mean full-depth summer circulation and transports at the northern periphery of the Atlantic Ocean in the 2000s. *J. Geophys. Res. Oceans* **117**, C01014 (2012).
26. Dickson, R. R. & Brown, J. The production of North Atlantic Deep Water: sources, rates, and pathways. *J. Geophys. Res. Oceans* **99**, 12,319–12,341 (1994).
27. Schott, F. A., McCreary, J. P. & Johnson, G. C. in *Earth's Climate: The Ocean–Atmosphere Interaction* (eds Wang, C. et al.) 261–304 (AGU, Washington DC, 2004).
28. Kostov, Y., Armour, K. C. & Marshall, J. Impact of the Atlantic meridional overturning circulation on ocean heat storage and transient climate change. *Geophys. Res. Lett.* **41**, 2108–2116 (2014).
29. Williams, R. G., Marshall, J. C. & Spall, M. A. Does Stommel's mixed layer "demon" work? *J. Phys. Oceanogr.* **25**, 3089–3102 (1995).
30. Capotondi, A., Alexander, M. A., Bond, N. A., Curchitser, E. N. & Scott, J. D. Enhanced upper ocean stratification with climate change in the CMIP3 models. *J. Geophys. Res. Oceans* **117**, C04031 (2012).
31. Heuzé, C., Heywood, K. J., Stevens, D. P. & Ridley, J. K. Changes in global ocean bottom properties and volume transports in CMIP5 models under climate change scenarios. *J. Clim.* **28**, 2917–2944 (2015).
32. Falina, A. et al. On the cascading of dense shelf waters in the Irminger Sea. *J. Phys. Oceanogr.* **42**, 2254–2267 (2012).
33. Germe, A., Houssais, M.-N., Herbaut, C. & Cassou, C. Greenland Sea sea ice variability over 1979–2007 and its link to the surface atmosphere. *J. Geophys. Res. Oceans* **116**, C10034 (2011).
34. Peralta-Ferriz, C. & Woodgate, R. A. Seasonal and interannual variability of pan-arctic surface mixed layer properties from 1979 to 2012 from hydrographic data, and the dominance of stratification for multiyear mixed layer depth shoaling. *Prog. Oceanogr.* **134**, 19–53 (2015).
35. Kuhlbrodt, T., Titz, S., Feudel, U. & Rahmstorf, S. A simple model of seasonal open ocean convection. *Ocean Dynam.* **52**, 36–49 (2001).
36. McCartney, M. S. & Talley, L. D. The subpolar mode water of the North Atlantic Ocean. *J. Phys. Oceanogr.* **12**, 1169–1188 (1982).
37. Trossman, D. S., Thompson, L. A., Kelly, K. A. & Kwon, Y.-O. Estimates of North Atlantic ventilation and mode water formation for winters 2002–06. *J. Phys. Oceanogr.* **39**, 2600–2617 (2009).
38. Thomas, M. D. & Fedorov, A. V. The eastern subtropical Pacific origin of the equatorial cold bias in climate models: a Lagrangian perspective. *J. Clim.* **30**, 5885–5900 (2017).
39. Burkholder, K. C. & Lozier, M. S. Subtropical to subpolar pathways in the North Atlantic: deductions from Lagrangian trajectories. *J. Geophys. Res. Oceans* **116**, C07017 (2011).
40. BrodeauL.. & Koenigk, T. Extinction of the northern oceanic deep convection in an ensemble of climate model simulations of the 20th and 21st centuries. *Clim. Dynam.* **46**, 2863–2882 (2016).
41. Xu, L., Xie, S.-P. & Liu, Q. Mode water ventilation and subtropical countercurrent over the North Pacific in CMIP5 simulations and future projections. *J. Geophys. Res. Oceans* **117**, C12009 (2012).
42. Lazier, J. The renewal of Labrador Sea water. *Deep Sea Res. Oceanogr. Abstr.* **20**, 341–353 (1973).
43. Våge, K. et al. Surprising return of deep convection to the subpolar North Atlantic Ocean in winter 2007–2008. *Nat. Geosci.* **2**, 67–72 (2009).
44. Piron, A., Thierry, V., Mercier, H. & Caniaux, G. Argo float observations of basin-scale deep convection in the Irminger sea during winter 2011–2012. *Deep Sea Res. I* **109**, 76–90 (2016).
45. Sévellec, F., Fedorov, A. V. & Liu, W. Arctic sea-ice decline weakens the Atlantic Meridional Overturning Circulation. *Nat. Clim. Change* **7**, 604–610 (2017).
46. Yang, H. et al. Intensification and poleward shift of subtropical western boundary currents in a warming climate. *J. Geophys. Res. Oceans* **121**, 4928–4945 (2016).
47. Bakker, P. et al. Fate of the Atlantic Meridional Overturning Circulation: Strong decline under continued warming and Greenland melting. *Geophys. Res. Lett.* **43**, 12 (2016).

48. Gillard, L. C., Hu, X., Myers, P. G. & Bamber, J. L. Meltwater pathways from marine terminating glaciers of the Greenland ice sheet. *Geophys. Res. Lett.* **43**, 10 (2016).
49. Exarchou, E., Kuhlbrodt, T., Gregory, J. M. & Smith, R. S. Ocean heat uptake processes: a model intercomparison. *J. Clim.* **28**, 887–908 (2015).
50. Pérez, F. F. et al. Atlantic Ocean CO_2 uptake reduced by weakening of the meridional overturning circulation. *Nat. Geosci.* **6**, 146–152 (2013).
51. Winton, M., Griffies, S. M., Samuels, B. L., Sarmiento, J. L. & Frölicher, T. L. Connecting changing ocean circulation with changing climate. *J. Clim.* **26**, 2268–2278 (2013).

Acknowledgements

We are deeply grateful to A. Voldoire and R. Séférian (CNRM, Toulouse, France) for making the model outputs from the different simulations available, and providing guidance on their use.

Author contributions

C.L. and M.T. designed the study. M.T. performed the Lagrangian analysis. C.L. and M.T. analysed the results. C.L. wrote the manuscript with input from M.T.

Competing interests

The authors declare no competing interests.

Additional information

Supplementary information is available for this paper at https://doi.org/10.1038/s41558-018-0316-5.

Reprints and permissions information is available at www.nature.com/reprints.

Correspondence and requests for materials should be addressed to C.L.

Publisher's note: Springer Nature remains neutral with regard to jurisdictional claims in published maps and institutional affiliations.

Methods

The simulations used in this study were performed with the coupled climate model CNRM–CM5.2. It includes the ORCA1 configuration[52] based on the NEMO ocean model[53], a sea ice component based on the GELATO model[54] and the ARPEGE-Climat model for the atmospheric component[55]. The model has an atmospheric horizontal resolution of 1.4° both in latitude and longitude and 31 vertical levels, while the ocean and sea ice components use a tri-polar grid with a nominal horizontal resolution of 1° and 42 unevenly spaced levels in the vertical. The CNRM model does not include any dynamical representation of the terrestrial ice sheet and thus does not include the possible effect of Greenland Ice Sheet melting on the AMOC projected changes. For the ocean component, parameterizations include an along-isopycnal and a horizontal Laplacian operator for the lateral diffusivity and viscosity, respectively, and an energy- and enstrophy-conserving scheme for the momentum advection[56]. Eddies are parameterized by the Gent and McWilliams[57] adiabatic mixing scheme with a latitudinally varying thickness diffusion coefficient. The mixed-layer dynamics are parameterized using the turbulent kinetic energy closure scheme[58]. A full description and basic evaluation of the model can be found in Voldoire et al.[20]. In particular, the model reproduces reasonably well the mean vertical structure of the AMOC at 26° N when compared against observations from the RAPID array (Fig. 2a), although the model transport is weaker than observed. As part of the CORE II exercise, the mean and interannual variability of the AMOC simulated by the ocean–sea ice components of the different CMIP5 models forced with the same atmospheric reanalysis have been compared[59,60]. The mean AMOC simulated by the CNRM model in forced mode (16.5 Sv) is within the range of values most commonly simulated by the different models, and its interannual variations share many similarities with the other models. As part of the same model intercomparison exercise, the behaviour of the ocean and sea ice components of the CNRM model in the Arctic Basin has also been extensively evaluated[61–63], giving support to the ability of the model to simulate present-day conditions and future changes in this region. Moreover, the CNRM model is able to reproduce realistic patterns of the March climatology MLD and stratification (see Supplementary Fig. 1) when compared against observation-based climatologies, and the performances of the model (in its previous version designed for CMIP5) regarding these features are again within the range of values commonly found in CMIP5 models[23,31].

In the present study, two simulations are analysed. The first is a 130-year control integration (labelled CTRL) in which greenhouse gases are kept constant at pre-industrial concentrations (285 ppm). The second simulation (labelled $4\times CO_2$) is initialized from the same initial conditions as the CTRL simulation, but the simulation is this time run for 130 years with constant atmospheric concentration of CO_2 four times higher than the pre-industrial level. The idealized forcing allows for a clearer assessment of the response to radiative forcing than a simulation with more complicated scenarios of future radiative forcing, such as those used as part of the Intergovernmental Panel on Climate Change model intercomparison. Here, the level of CO_2 is ~30% weaker than the value at which the least conservative scenario (RCP8.5) plateaus. For the present study, we use monthly mean output from 60 years of each simulation (years 70 to 129), allowing for an initial strong adjustment period of the ocean state. Yet, we acknowledge that the simulations used in this study are much shorter than the time required to bring the ocean–atmosphere system into a fully equilibrated state.

We also make use of the particle-tracking tool, ARIANE[64], to calculate Lagrangian trajectories from the model output velocity fields. We follow closely the methodology presented in Thomas et al.[18] to perform our Lagrangian experiments. Briefly, we limit our domain of investigation to the North Atlantic and Arctic basins, bounded between a zonal section across the Atlantic at 10° N and the Bering Strait (65° N in the Pacific). To describe the full southward flow in the deep Atlantic Basin, particles have been seeded each month of the 60-year period in every grid cell along the 10° N Atlantic cross-section, and then run backward in time until they exit the domain, either back at 10° N or at the Bering Strait. As the timescale for North Atlantic water to complete a full overturning circuit can greatly exceed the 60 years of model output available here, we loop over 10 cycles (600 years in total) of the model output, after which almost all of the approximately 1.2 million particles were intercepted. In this manner, if enough particles are seeded, the full AMOC streamfunction can be reconstructed[65] and the discrepancies between the AMOC estimates from the Eulerian fields and the Lagrangian method are small (see Supplementary Figs. 2 and 3). By then tagging the particles at the location where they were last subducted from the mixed layer, the AMOC streamfunction can be decomposed according to its different geographical sources of ventilated water. The mixed layer is defined by a density threshold of 0.01 kg m^{-3} compared to the surface density. The use of monthly mean model fields for the MLD determination and the Lagrangian analysis means that high-frequency fluctuations of the MLD and the subduction processes resulting, for instance, from high-frequency atmospheric forcing[66] are not fully sampled by the particles in this study. Particles released within the mixed layer along the section at 10° N are tagged immediately on seeding and their small associated transport is thus incorporated to the integrated contribution from the subtropical region. In the following, we also omit the 'Bering component', which corresponds to the small contributions of waters from the Bering Strait that never pass through the mixed layer before reaching 10° N, and which contributes 0.04 Sv and 0.3 Sv to the CTRL and $4\times CO_2$ AMOCs, respectively. The sensitivity of the results to looping is small, and discussed extensively in Thomas et al.[18], along with additional discussion on the different sources of uncertainty associated with the methodology. In particular, we acknowledge that our results are probably affected by the use of monthly averaged fields to perform the Lagrangian analysis (ignoring in this way the potential effect of the nonlinear terms in the momentum equations)[67], although previous studies have suggested that the errors arising from the use of monthly averaged output from a non-eddy resolving model (such as the CNRM model) are quite small[68].

Code availability. NEMO code is available at http://www.nemo-ocean.eu and ARIANE at http://www.umr-lops.fr/Technologies/Logiciels/ARIANE. Specific configurations can be provided upon request.

Data availability

The data sets generated and analysed during the current study are available upon request from the corresponding author.

References

52. Hewitt, H. et al. Design and implementation of the infrastructure of HadGEM3: The next-generation Met Office climate modelling system. *Geosci. Model Dev.* **4**, 223–253 (2011).
53. Madec, G. *NEMO Ocean Engine, Note du Pôle Modélisation 27* (Institut Pierre-Simon Laplace, 2008).
54. Salas y Mélia, D. A global coupled sea ice–ocean model. *Ocean Model.* **4**, 137–172 (2002).
55. Déqué, M., Dreveton, C., Braun, A. & Cariolle, D. The ARPEGE/IFS atmosphere model: a contribution to the French community climate modelling. *Clim. Dyn.* **10**, 249–266 (1994).
56. Le Sommer, J., Penduff, T., Theetten, S., Madec, G. & Barnier, B. How momentum advection schemes influence current topography interactions at eddy permitting resolution. *Ocean Model.* **29**, 1–14 (2009).
57. Gent, P. R. & McWilliams, J. C. Isopycnal mixing in ocean circulation models. *J. Phys. Oceanogr.* **20**, 150–160 (1990).
58. Blanke, B. & Delecluse, P. Variability of the tropical Atlantic ocean simulated by a general circulation model with two different mixed-layer physics. *J. Phys. Oceanogr.* **23**, 1363–1388 (1993).
59. Danabasoglu, G. et al. North Atlantic simulations in Coordinated Ocean-ice Reference Experiments phase II (CORE-II). Part I: Mean states. *Ocean Model.* **73**, 76–107 (2014).
60. Danabasoglu, G. et al. North Atlantic simulations in Coordinated Ocean-ice Reference Experiments phase II (CORE-II). Part II: Inter-annual to decadal variability. *Ocean Model.* **97**, 65–90 (2016).
61. Ilicak, M. et al. An assessment of the Arctic Ocean in a suite of interannual CORE-II simulations. Part III: Hydrography and fluxes. *Ocean Model.* **100**, 141–161 (2016).
62. Wang, Q. et al. An assessment of the Arctic Ocean in a suite of interannual CORE-II simulations. Part I: Sea ice and solid freshwater. *Ocean Model.* **99**, 110–132 (2016).
63. Wang, Q. et al. An assessment of the Arctic Ocean in a suite of interannual CORE-II simulations. Part II: Liquid freshwater. *Ocean Model.* **99**, 86–109 (2016).
64. Blanke, B. & Raynaud, S. Kinematics of the Pacific Equatorial Undercurrent: an Eulerian and Lagrangian approach from GCM results. *J. Phys. Oceanogr.* **27**, 1038–1053 (1997).
65. Blanke, B., Arhan, M., Speich, S. & Pailler, K. Diagnosing and picturing the North Atlantic segment of the global conveyor belt by means of an ocean general circulation model. *J. Phys. Oceanogr.* **32**, 1430–1451 (2002).
66. Holdsworth, A. M. & Myers, P. G. The influence of high-frequency atmospheric forcing on the circulation and deep convection of the Labrador Sea. *J. Clim.* **28**, 4980–4996 (2015).
67. Van Sebille, E. et al. Lagrangian ocean analysis: Fundamentals and practices. *Ocean Model.* **121**, 49–75 (2018).
68. Valdivieso Da Costa, M. & Blanke, B. Lagrangian methods for flow climatologies and trajectory error assessment. *Ocean Model.* **6**, 335–358 (2004).